

This work was written as part of one of the author's official duties as an Employee of the United States Government and is therefore a work of the United States Government. In accordance with 17 U.S.C. 105, no copyright protection is available for such works under U.S. Law.

Public Domain Mark 1.0

<https://creativecommons.org/publicdomain/mark/1.0/>

Access to this work was provided by the University of Maryland, Baltimore County (UMBC) ScholarWorks@UMBC digital repository on the Maryland Shared Open Access (MD-SOAR) platform.

Please provide feedback

Please support the ScholarWorks@UMBC repository by emailing scholarworks-group@umbc.edu and telling us what having access to this work means to you and why it's important to you. Thank you.

Observed effects of particles nonsphericity on the retrieval of marine and desert dust aerosol optical depth by lidar

G.P. Gobbi ^{a,*}, F. Barnaba ^b, M. Blumthaler ^c, G. Labow ^d,
J.R. Herman ^d

^a*Istituto per l'Inquinamento Atmosferico CNR, Rome, Italy*

^b*Istituto di Fisica dell' Atmosfera CNR, Rome, Italy*

^c*Institute of Medical Physics, University of Innsbruck, Innsbruck, Austria*

^d*NASA, Goddard Space Flight Center, Greenbelt, MD, USA*

Received 5 June 2001; accepted 14 August 2001

Abstract

Polarization lidar observations of maritime and Saharan dust aerosols collected at Crete (35.5°N–23.7°E) during the May 1999 PAUR II campaign are discussed. Lidar traces are inverted and integrated to provide aerosol optical depth at 532 nm. Two model relationships linking together aerosol backscatter and extinction coefficients are employed to perform such an inversion: one obtained employing the Mie theory, i.e., considering both maritime and dust particles as spheres, and a second one obtained by modeling dust particles as spheroids. The resulting two sets of aerosol optical depths are then compared to the ones measured by two independent, ground-based sunphotometers. These comparisons show that a good agreement exist between both lidar inversions and photometer-derived aerosol optical depths. However, the lidar retrieval employing the nonspherical model leads to a better agreement with photometric data when desert dust is observed. Average lidar–sunphotometer aerosol optical depth differences range between 12% and 24%. These values are comparable and sometimes smaller than ones observed to occur between the two sunphotometers employed in this exercise. © 2002 Elsevier Science B.V. All rights reserved.

Keywords: Desert dust; Nonspherical aerosol scattering; Lidar

* Corresponding author. Istituto di Fisica dell' Atmosfera CNR, Via Fosso del Cavaliere, 100, 00133 Rome, Italy. Tel.: +39-06-4993-4343; fax: +39-06-2066-0291.

E-mail addresses: gobbi@ifa.rm.cnr.it (G.P. Gobbi), francesca.barnaba@ifa.rm.cnr.it (F. Barnaba), Mario.Blumthaler@uibk.ac.at (M. Blumthaler), labow@qhearts.gsfc.nasa.gov (G. Labow).

1. Introduction

Large uncertainties exist about the impact of mineral dust (of both anthropogenic and natural origin) on the Earth's radiative budget and consequently on its climate. These uncertainties are a consequence of our poor knowledge of dust optical properties (as short-wave and long-wave scattering and absorption coefficients) and of its regional and altitude location (Lacis and Mishchenko, 1995; Sokolik and Toon, 1996; Hansen et al., 1997; Kaufman et al., 2001). In fact, mineral dust can lead to opposite radiative effects, i.e., a warming of the planet, with respect to sulphate aerosols (e.g., Hansen et al., 1997). The magnitude of such a heating has been shown to increase for increasing values of the: (1) aerosol imaginary refractive index; (2) dust layer altitude; (3) albedo of the underlying surface; (4) cloud-free portion of the atmosphere (Liao and Seinfeld, 1998; Quijano et al., 2000). In this respect, polarization lidars represent a unique and affordable tool to retrieve the altitude-resolved information on both aerosol nature and scattering properties, and on cloud extent and frequency needed to better evaluate the radiative effects of these particles (e.g., Gobbi et al., 2000).

Inversion of the single-wavelength lidar signal to derive vertically resolved aerosol extinction $\sigma_a(z)$ or backscatter $\beta_a(z)$ coefficients requires the knowledge of the relationship between $\beta_a(z)$ and $\sigma_a(z)$ since both unknowns appear in the relevant equation (e.g., Measures, 1984; Klett, 1985). Such a relationship (often indicated as lidar ratio $R_L = \sigma_a / \beta_a$) is poorly known, therefore, it is often taken as a constant value, typical of the observed aerosols along the whole lidar trace. However, it has been shown (Kovalev, 1995) that the latter assumption can lead to largely inaccurate estimates of the aerosol extinction when employed in nonhomogeneous, that is real, atmospheres. Ways to actually measure the relationship between aerosol extinction and backscatter coefficients are provided by the use of Raman or high spectral resolution lidars (e.g., Ansmann et al., 1992; Piironen and Eloranta, 1994). However, these techniques are more expensive and less portable than simple elastic backscatter lidars. In this latter case, a statistical model approach providing the relationship $\sigma_a = f(\beta_a)$ to determine aerosol extinction by the inversion of the single-wavelength lidar trace has been shown to be quite effective in the case of stratospheric (Gobbi, 1995) and maritime–desert dust aerosols (Barnaba and Gobbi, 2001).

To determine such relationships, these models adopt a Monte Carlo technique: for each aerosol type (e.g., maritime, desert) optical properties are computed for a large (20,000) set of size distributions and refractive indices, taken as representative of all the possible size distributions and compositions this type of aerosols can exhibit. This is achieved by randomly varying the distribution parameters (modal radii, widths, number concentrations, refractive indices) within boundaries spanning the largest variability experimentally observed in nature and reported in the scientific literature (e.g., Gobbi, 1995). The scatter plot of the σ_a vs. β_a obtained by these optical computations is then fitted by polynomials (in log–log coordinates) which provide the analytical relationship $\sigma_a = f(\beta_a)$ to be used in the lidar inversion process. In spite of its simple approach, implementation of the model is quite complex and the reader is referred to the original papers for a more thorough description of its rationale and results.

Here we shall employ the aerosol model relationships $\sigma_a = f(\beta_a)$ found by Barnaba and Gobbi (2001) for the ensemble of maritime and dust aerosols, to obtain altitude-resolved extinction and total optical depth from elastic backscatter lidar observations of desert dust and maritime aerosols collected at Crete, during the spring of 1999. Use of the maritime–desert aerosol model to invert the Crete measurements is justified by the observation site being located in the upwind portion of the island and at approximately 100 m from the coast. In fact, Barnaba and Gobbi (2001) provide two functional relationships linking together aerosol extinction and backscatter: (1) one obtained by means of Mie theory (both maritime and dust aerosol were assumed to be spherical); (2) a second one obtained by employing for the desert dust the scattering computations for dust-like, polydisperse, randomly oriented prolate and oblate spheroids performed by Mishchenko et al. (1997). In this latter case, the model addresses maritime aerosols as spherical particles and dust grains as spheroids. In this paper, we will then proceed to the evaluation of the performance of the two model relationships by comparing the lidar-derived aerosol optical depths ($\text{AOD} \equiv \tau$) against AOD measurements obtained by two different ground-based sunphotometers.

2. Methods

Observations employed in this work have been collected during the European Union Photochemical Activity and Ultraviolet Radiation (PAUR II) campaign, which took place at Crete in May 1999. Amongst several other instruments, two sunphotometers, one from the University of Innsbruck (UI) and the second from NASA Goddard, together with a polarization lidar from CNR Rome participated in the campaign with the goal of observing aerosol spectral extinction and vertical displacement. The two sunphotometers were located at the same site in Kolimbari (35.533°N–23.783°E, 15 m m.s.l.), approximately 10 km east of the lidar, which was located at Nopigia (35.509°N–23.722°E, 30 m m.s.l.). Characteristics of the instruments are reported hereafter.

2.1. The lidar system

The VEHICLE-mounted Lidar System (VELIS) employed for these observations is a compact, mobile lidar designed to provide day and night-time profiles of atmospheric aerosols from 150 m up to the lower stratosphere, with 75 m vertical resolution. This goal is achieved by adopting a two-telescope configuration, a large field-of-view one (4 mrad) for the near range (150–2000 m) and the second for the far range (1.5–25 km). The lidar emitter is based on a frequency doubled (532 nm) Nd:YAG laser, generating plane-polarized, 100-mJ pulses at 15 Hz. The atmospheric backscatter signal is detected by photomultipliers and digitized by means of 10-bit A/D converters in the near range channels and by photon counting devices in the far range channels. Daylight observations employed in this paper are the result of 5-min (4500 laser shots) time averages. At each receiver, both parallel S_{\parallel} and perpendicular S_{\perp} polarization signals (with respect to the polarized laser emission) are recorded. Since spherical particles do not depolarize while nonspherical particles introduce some degree of depolarization in

the light they backscatter, this technique allows for discrimination of spherical (liquid) vs. nonspherical (solid) particles by evaluating the linear depolarization ratio $D = S_{\perp}/S_{\parallel}$ (e.g., Gobbi, 1998).

As mentioned above, inversion of the VELIS observations is performed twice, that is by employing two model-derived relationships $\sigma_a = f(\beta_a)$ to numerically solve the single wavelength lidar equation. These two relationships are in the form of seventh order polynomials, one describing the $\sigma_a = f(\beta_a)$ behaviour for the ensemble of spherical maritime and spherical desert aerosols, the other describing the $\sigma_a = f(\beta_a)$ behaviour for the ensemble of spherical maritime and nonspherical desert aerosols (Barnaba and Gobbi, 2001). Since both variables σ_a and β_a appear in the lidar equation, an iteration-convergence procedure is adopted in solving it: (1) the lidar trace is calibrated against a model atmosphere at an aerosol-free point; (2) the aerosol backscatter β_a at each measurement point (75 m vertical resolution) is determined; (3) the aerosol extinction σ_a at each measurement point is determined by the model on the basis of the aerosol backscatter β_a computed at step 2; (4) at each measurement point, the signal is corrected for aerosol and molecular extinction encountered below that point; (5) steps 1–4 are iterated until convergence is reached.

When employing the nonspherical aerosol model, cases of mixed-phase aerosols (dust plus liquid particles) are also considered. In this case, the depolarization information is used to weigh the percent of nonspherical vs. spherical model to use. This algorithm is implemented as follows: σ_a is obtained by the spherical model alone when $D \leq 1.4\%$ and by the nonspherical model alone when $D \geq 42\%$. This is because during PAUR II, typical depolarization of liquid aerosols was below the molecular value of $D \leq 1.4\%$, while typical depolarization of desert dust was observed to be $D \approx 42\%$ (e.g., Gobbi et al., 2000). Intermediate cases, i.e., coexistence of dust and liquid particles, are weighed according to the ratio $D/\{[(R_{\parallel} - 1) \times 41 + 1.4]/R_{\parallel}\}$ between the actually measured depolarization D and the one expected from a dust + molecules atmosphere with relative weights of $(R_{\parallel} - 1)$ and 1, respectively. Here $R_{\parallel} = [(\beta_a + \beta_m)/\beta_m]$ represents the parallel channel-derived backscatter ratio, with β_a and β_m being the aerosol and molecular backscatter coefficients, respectively.

Output of this analysis applied to each lidar measurement are two profiles of aerosol extinction which are then integrated up to the tropopause to provide the aerosol optical depth according to the relevant model. The expected error of the lidar-derived AOD ranges between 20% and 40% (Barnaba and Gobbi, 2001). As previously indicated, the lowermost 150 m of the atmosphere are not fully observed by the lidar due to still incomplete superposition between the telescope field of view and the laser beam. In our analysis, this is accounted for by correcting the signal recorded at the lower levels for overlapping losses. Therefore, the VELIS aerosol profile is assumed to be representative of the whole atmosphere.

2.2. The University of Innsbruck spectroradiometer

The spectroradiometer of the group from the Institute for Medical Physics, University of Innsbruck (UI), is a double monochromator (BENTHAM DTM300, UK) with a bandwidth of 0.43 nm (full width at half maximum). Each scan covers the wavelength

range from 290 to 600 nm with steps of 0.25 nm, in about 5 min. The spectroradiometer is calibrated against a 1000-W halogen lamp, traceable to Physikalisch-Technische Bundesanstalt, Germany. The overall uncertainty of the calibration is estimated to be about $\pm 5\%$. The instrument has two entrance slits, one for measurements of global irradiance with a Teflon diffuser, which is especially designed to give an angular response very close to the ideal cosine response. The second input port is fitted with a 6-m quartz fibre to a small telescope with a field of view of about 1.5° , which is mounted on a custom-made suntracker. This allows for spectral measurements of direct sun irradiance, from which total column ozone and aerosol optical depth in the wavelength range 290–600 nm are determined (Huber et al., 1995). The absolute uncertainty of the aerosol optical depth measurements is estimated to be less than about ± 0.04 . The spectral dependence of aerosol optical depth (τ) is fitted by a power law according to the Angstrom formula:

$$\tau = A\lambda^{-\alpha} \quad (1)$$

where λ is the wavelength in micrometers, while α and A are fit parameters (α =Angstrom coefficient). This fit is employed to provide the AOD value at the lidar wavelength of 532 nm. The uncertainty of the calculated parameter α is estimated to be less than about ± 0.2 .

2.3. The NASA Goddard sunphotometer

The sun photometer used by the NASA Goddard group is a CIMEL spectral radiometer. The instrument makes direct Sun measurements every 15 min at 340, 380, 440, 500, 670, 870, 940 and 1020 nm (e.g., Holben et al., 1998). The bandpass of the filters are as follows: 2 nm at 340 nm, 4 nm at 380 nm, 10 nm from 440 to 1020 nm. Each direct sun measurement takes 8 s to scan across all eight wavelengths using a motor-driven filter wheel. The instrument's field of view is 1.2° . The uncertainty of the measured AOD values due to the uncertainty in defining the extraterrestrial flux is better than 0.01–0.02. The total uncertainty in the AOD measurements due to additional errors (Eck et al., 1999) is estimated to be 0.01–0.02. However, there can exist a small bias due to forward scattered diffuse radiation (due to the instrument 1.2° field of view) in the presence of desert dust. If the dust particles have an effective radius of $1.75 \mu\text{m}$, the measured optical depths would be $\sim 0.7\%$ below the actual values.

During the PAUR II campaign, the instrument was in operation between May 6 and 26, 1999, but hardware problems reduced the quality of data collected before May 12.

2.4. Comparison of data

Lidar-estimated and sunphotometer AOD observations are all compared at the lidar wavelength of 532 nm. Two examples of Angstrom fits to the UI spectral AOD measurements are shown in Fig. 1 for the dates of May 11 and 19, 1999. These days correspond to a maritime aerosol load and to heavy Saharan dust load, respectively (e.g., Gobbi et al., 2000). The Angstrom coefficients obtained from the fitting of the

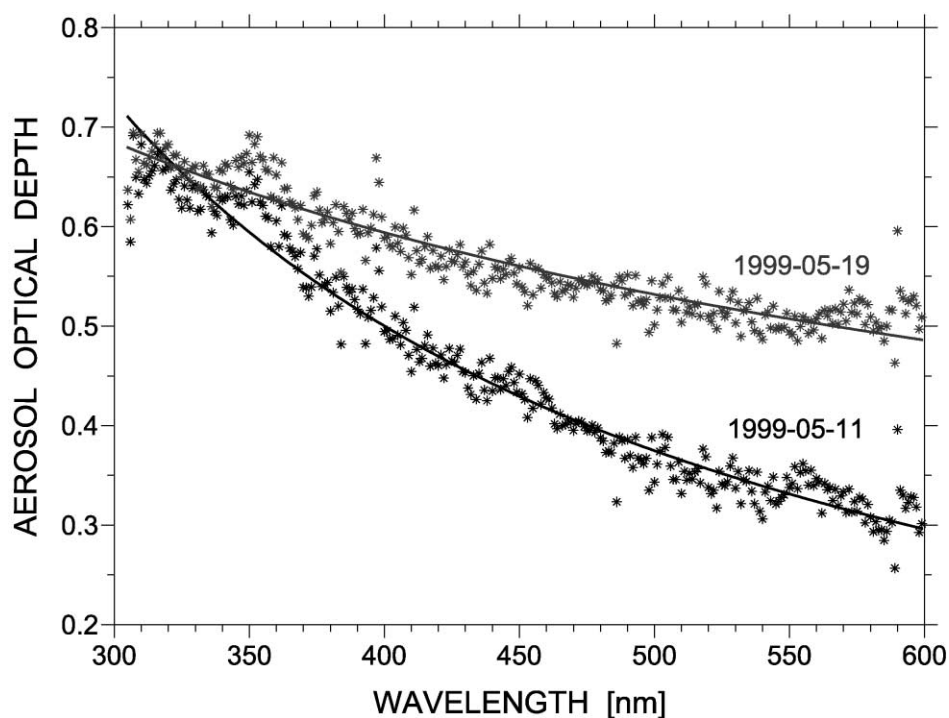


Fig. 1. Spectral behaviour of the aerosol optical depth as measured by the University of Innsbruck BENTHAM spectrophotometer on May 11 and 19, 1999. Best fits employing the Angstrom formula are also plotted.

spectroradiometer data are $\alpha = 1.29$ and 0.50 , respectively. These values well characterize the change the Angstrom coefficient undergoes when switching from small, submicron aerosols to larger supermicron ones. The 532-nm AOD resulting from such fits is $\tau = 0.35$ on May 11 and $\tau = 0.52$ on May 19, respectively.

Angstrom coefficients derived from the UI observations are also employed to convert the NASA 500-nm AOD observations into 532-nm ones. This is because spectrophotometric measurements are assumed to provide a better description of the Angstrom coefficient than the discrete wavelength observations of the NASA sunphotometer. In the case UI and NASA observations do not coincide in time, α is estimated by time interpolation of UI-derived values, provided that the maximum time lag between the UI and the NASA observations is less than 2 h. However, the comparison between the two sunphotometer observations discussed hereafter was performed only when the time lag between their measurements was less than 30 min.

Due to the distance between the lidar and the sunphotometers sites (approximately 10 km), comparison between lidar and photometers measurements was performed only when the time lag was less than 1 h. In this respect, the agreement between the two sunphotometers is somewhat more likely to be found than the lidar–sunphotometer one. Both VELIS and UI measurements employed here were collected in clear sky

conditions, i.e., lidar and visual controls were performed to exclude observations affected by the presence of any type of clouds. Conversely, the automated NASA sunphotometer operated continually and cloud-free conditions are assumed on the basis of the near-coincidence in time with the UI cloud-free observations.

3. Results and discussion

The time evolution of the aerosol optical depth at 532 nm as measured by the two sunphotometers and by VELIS (spherical and nonspherical model) during PAUR II is reported in Fig. 2a and b, respectively. The observational period common to the three instruments begins on May 6, ending on May 20, 1999. Analysis of this period shows the aerosol optical depth to increase from a minimum value of $\tau \approx 0.1$ on May 6 to a

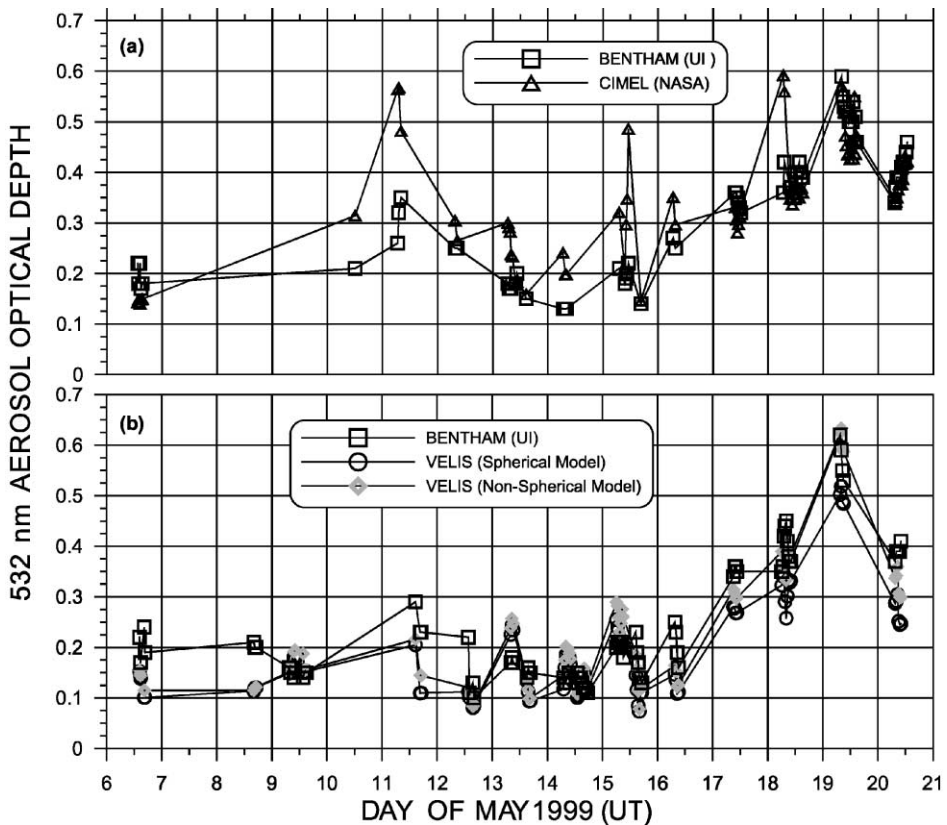


Fig. 2. Time evolution of the 532-nm aerosol optical depth (AOD) as obtained by: (a) the University of Innsbruck BENTHAM spectrophotometer (open squares) and the NASA CIMEL sunphotometer (open triangles), and (b) the University of Innsbruck BENTHAM spectrophotometer (open squares) and the VELIS lidar employing the spherical (open circles) and nonspherical (open diamonds) inversion schemes.

maximum $\tau \approx 0.65$ on May 19. Backtrajectory analysis, together with a marked increase in depolarization, revealed the sharp increase in AOD recorded in the period 15–22 of May to be associated to a Saharan dust transport, mainly originating from southern Algeria. During the Saharan event, the lidar observed the dust layer to extend up to 10 km, with most of the optical depth building up above 1 km altitude. Conversely, most of the aerosol extinction was observed to take place below the 2-km level during minimum load conditions (Gobbi et al., 2000). This different behaviour is depicted by the two lidar profiles reported in Fig. 3. The AOD was finally observed to decrease back to minimum values of $\tau \approx 0.1$ after May 23, 1999.

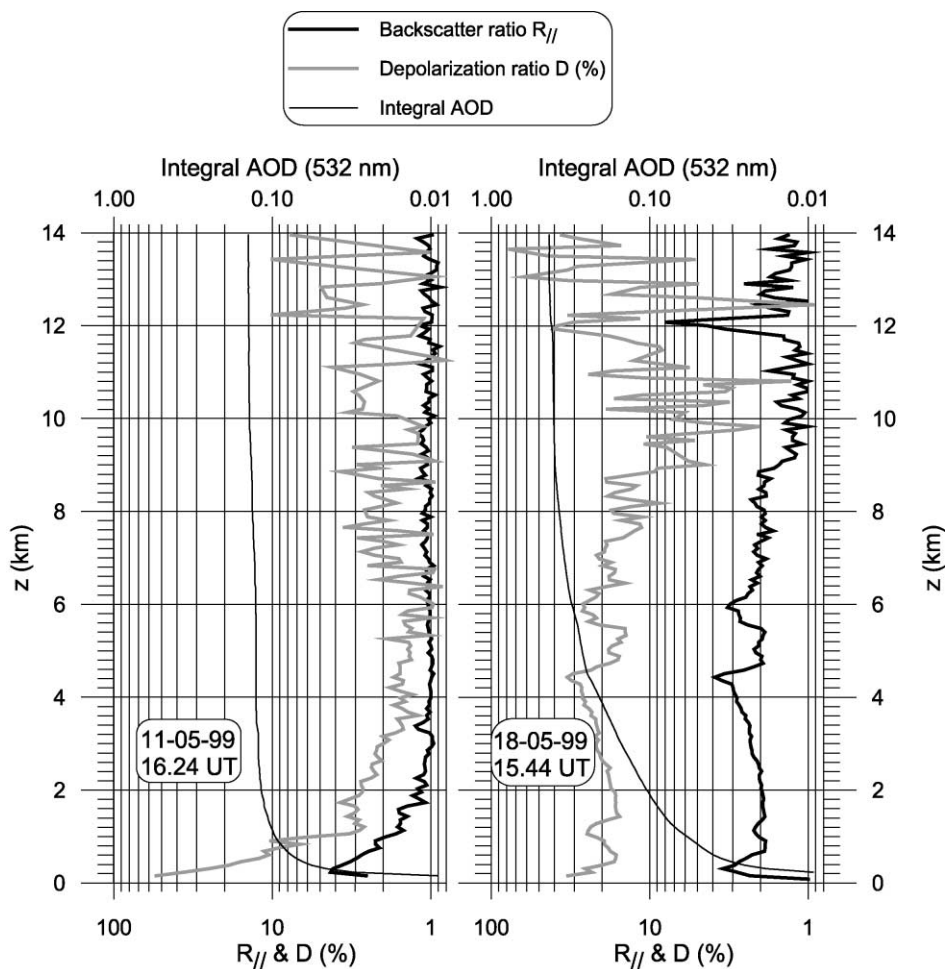


Fig. 3. VELIS lidar profiles obtained before (May 11) and during (May 18) the Saharan dust event. Each box reports the lidar backscatter and depolarization ratio (thick black and grey line, respectively) and the integral from ground to z of the 532-nm aerosol extinction (thin black line).

The time evolution of AOD differences between the three data sets is presented in Fig. 4. Differences are computed by taking the UI record as a reference and by subtracting it from the corresponding values retrieved by the NASA sunphotometer (Fig. 4a) and VELIS (employing both spherical and nonspherical model, Fig. 4b). These plots do not show any large systematic difference between the three instrument results. In both plots, differences tend to become slightly negative during the dust event period (15–20 May). As expected, during this period the nonspherical model shows larger extinction values and leads to a better agreement.

Statistics of the comparisons between the three data sets is summarised in Table 1. Here root mean square AOD differences $|\overline{d\tau}|$, relative differences $|d\tau|/\tau$ and the relevant standard deviations are reported. Comparisons are made for the whole period (May 6–20, 1999), for the minimum aerosol load period (May 6–14, 1999) and for the dust event period (May 15–20, 1999). This subdivision has been added to better isolate the effects of

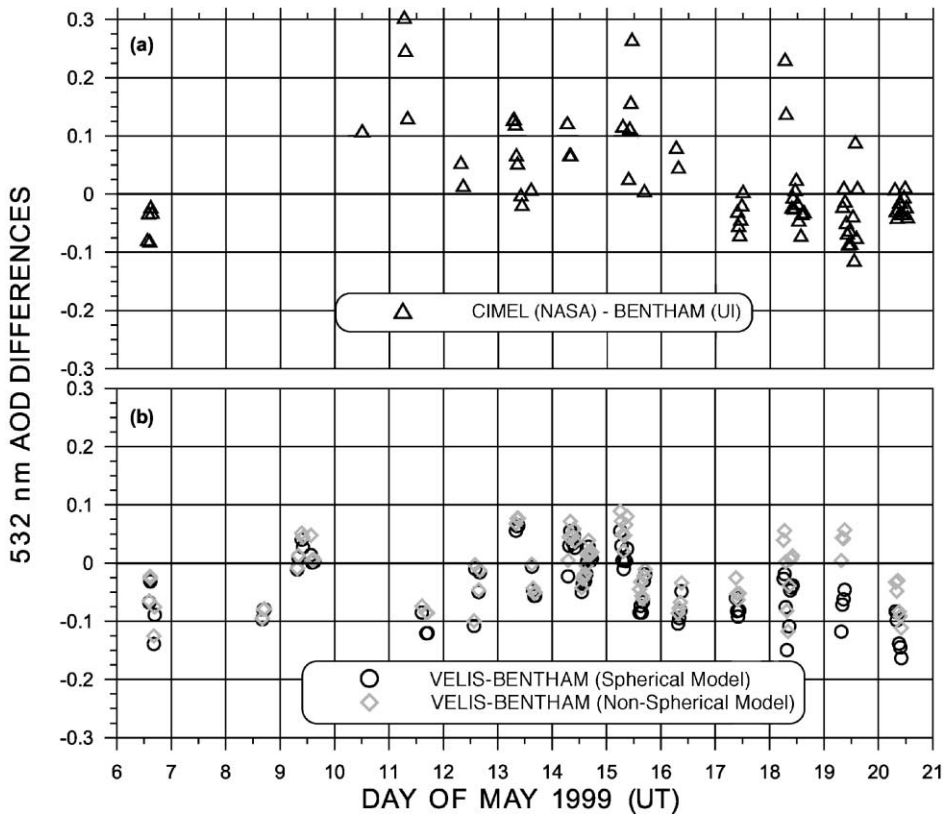


Fig. 4. Time evolution of the AOD differences as obtained by subtracting: (a) the University of Innsbruck BENTHAM observations from the NASA CIMEL ones (open triangles), and (b) the University of Innsbruck BENTHAM observations from the VELIS AOD estimates obtained by employing the spherical (open circles) and nonspherical (open diamonds) inversion schemes.

Table 1

Root mean square values and relevant standard deviations (s.d.) of differences $|\mathrm{d}\tau|$ and relative differences $|\mathrm{d}\tau|/\tau$ obtained by subtracting the University of Innsbruck AOD observations from the NASA sunphotometer and the VELIS lidar-derived (employing spherical (s) and nonspherical (ns) inversion schemes) observations

Datasets	$ \mathrm{d}\tau $ (\pm s.d.)						$ \mathrm{d}\tau /\tau$ (\pm s.d.)					
	May 6–14		May 15–20		May 6–20		May 6–14		May 15–20		May 6–20	
NASA–UI	23	0.081 ± 0.074	52	0.051 ± 0.053	75	0.061 ± 0.061	23	0.40 ± 0.30	52	0.16 ± 0.22	75	0.23 ± 0.27
VELIS(s)–UI	46	0.044 ± 0.035	40	0.071 ± 0.045	86	0.056 ± 0.042	46	0.25 ± 0.16	40	0.23 ± 0.14	86	0.24 ± 0.15
VELIS(ns)–UI	46	0.043 ± 0.031	40	0.050 ± 0.029	86	0.047 ± 0.030	46	0.25 ± 0.15	40	0.19 ± 0.12	86	0.22 ± 0.14
VELIS(s)–NASA	8	0.034 ± 0.037	50	0.077 ± 0.058	58	0.070 ± 0.057	8	0.17 ± 0.15	50	0.19 ± 0.13	58	0.19 ± 0.13
VELIS(ns)–NASA	8	0.027 ± 0.031	50	0.048 ± 0.040	58	0.045 ± 0.039	8	0.13 ± 0.13	50	0.12 ± 0.09	58	0.12 ± 0.09

The comparisons are performed for the full period (May 6–20, 1999) and for the the dust-free (May 6–14) and dust-laden (May 15–20) periods. Number of employed data points is printed in bold.

spherical vs. nonspherical model results on the lidar-retrieved AOD. Number of compared observations is also reported for each case.

Analysis of the AOD differences $|\Delta\tau|$ is useful in quantifying the average magnitude of the measurements discrepancy. Three general features result from this analysis: (1) lidar and sunphotometer-measured AOD are generally in good agreement; (2) in the presence of dust, both comparisons with the UI and NASA data show the lidar-estimated AOD to achieve a better agreement when the nonspherical model is employed; (3) mean differences $|\Delta\tau|$ between NASA and UI and between VELIS and UI aerosol optical depths are of the same order.

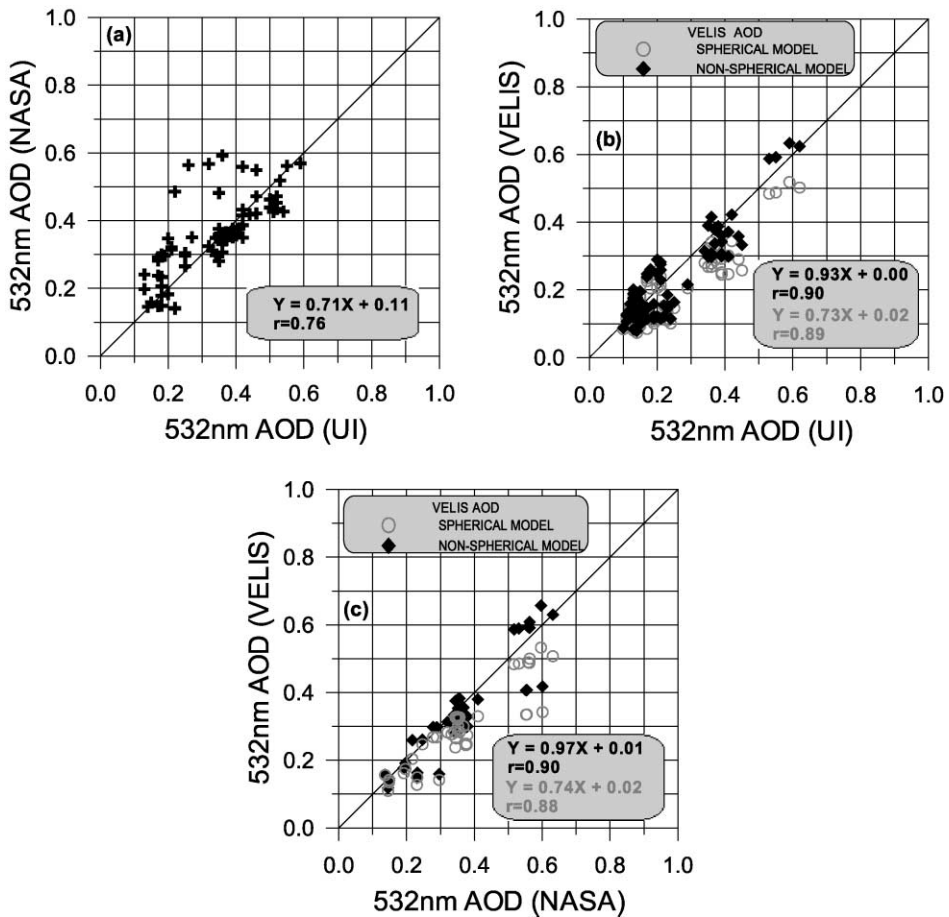


Fig. 5. Correlation analysis of the 532-nm aerosol optical depth as obtained by comparing: (a) the NASA CIMEL and the University of Innsbruck BENTHAM observations (crosses); (b) the University of Innsbruck BENTHAM and the VELIS observations obtained by employing the spherical (open circles) and nonspherical (full diamonds) inversion schemes; and (c) the NASA CIMEL and the VELIS observations obtained by employing the spherical (open circles) and nonspherical (full diamonds) inversion schemes.

In fact, for the two sunphotometers we find $|\mathrm{d}\tau| = 0.061 \pm 0.061$ over the whole period. This value decreases to $|\mathrm{d}\tau| = 0.051 \pm 0.053$ for the dust event period, when the NASA sunphotometer was performing better than at the beginning of the campaign. These differences are within the error bars of the two instruments reported above. When considering the lidar vs. sunphotometer comparisons, differences for the whole period range from $|\mathrm{d}\tau| = 0.045 \pm 0.039$ (nonspherical model VELIS–NASA data) to $|\mathrm{d}\tau| = 0.070 \pm 0.057$ (spherical model, VELIS–NASA). On average these differences are very similar to the ones found to exist between the two sunphotometers. It is also worth noticing that in background conditions, when nonspherical particles are not dominating, the spherical and the nonspherical models give, as expected, quite similar results.

The better performance of the nonspherical model clearly emerges during the dust event period. In fact, in the comparison of VELIS vs. UI observations in the period 15–20 May, the nonspherical model differences show $|\mathrm{d}\tau| = 0.050 \pm 0.029$, i.e., about 30% less than in the case of the spherical inversion where $|\mathrm{d}\tau| = 0.071 \pm 0.045$. Similarly, the comparison between VELIS nonspherical model results and NASA AODs during the same period shows $|\mathrm{d}\tau| = 0.048 \pm 0.040$, i.e., 38% less than in the spherical model case. In this respect, it is interesting to note that standard deviations of the lidar–sunphotometer comparisons are mostly smaller than the photometer–photometer ones and reach minimum values in the VELIS–UI comparisons.

In terms of mean percent deviation in AOD, it is worth noticing that the best agreement between the two sunphotometers (differences of about 16%) is found in the period 15–20 May. In the same period, VELIS–UI and VELIS–NASA differences decrease from 19–23% in the case of the spherical model, down to 12–19% in the case of the nonspherical one. Again, nonspherical model $|\mathrm{d}\tau|/\tau$ values are close to the sunphotometers ones and standard deviations are smaller indicating a smaller spread of the lidar–sunphotometer comparisons. To further quantify these results a correlation analysis of the three data sets has been performed and plotted in Fig. 5. In Fig. 5a the NASA–UI sunphotometers comparison shows a correlation coefficient $r = 0.76$ and a linear fit of $Y = 0.71X + 0.11$, i.e., the CIMEL tends to overestimate the AOD with respect to the BENTHAM. The situation does not substantially change when observations are reduced to the period 12–20 May, when the CIMEL was performing better. VELIS vs. sunphotometers correlations (Fig. 5b and c) show smaller intercept values (0.00–0.02) and higher correlation coefficients (0.88–0.90). This analysis, too, shows that the nonspherical model provides a much better agreement between the lidar-derived and both the sunphotometer-measured AOD. This is pointed out by the linear fit coefficients increasing from values of 0.73, 0.74 for the spherical model up to 0.93, 0.97 for the nonspherical one.

4. Conclusions

Lidar-derived and two sunphotometer-measured aerosol optical depth records collected at Crete in May 1999 have been compared to evaluate the performance of the two aerosol models used to retrieve AOD from the 532-nm lidar observations. Both these models provide functional relationships linking backscatter and extinction coefficients for the ensemble of maritime and desert dust particles, i.e., the aerosol types observed during the

campaign. However, the first model addresses both maritime and desert aerosols as spherical ones, while the second addresses the dust particles as randomly oriented spheroids (Barnaba and Gobbi, 2001). Aerosol extinction for the spherical and non-spherical assumption is then obtained from the lidar traces by iterative use of the relevant model relationship. Integration of the extinction profile up to 14 km provides the aerosol optical depths to be compared with the sunphotometer ones.

In the period May 15–May 20, 1999, when the NASA sunphotometer performed better and heavy dust loads were detected, comparisons between the two sunphotometer-measured AOD show an average difference of $|\mathrm{d}\tau| \approx 0.05$. This value falls within the sum of the instruments error bars $|\mathrm{d}\tau_{\text{UI}}| + |\mathrm{d}\tau_{\text{NASA}}| \approx 0.06$. Conversely, lidar–sunphotometer comparisons of the order of $|\mathrm{d}\tau| \approx 0.075$ when employing the spherical model and of the order of $|\mathrm{d}\tau| \approx 0.05$ in the case of the nonspherical one. In addition, standard deviations of the average differences $|\mathrm{d}\tau|$ are smaller in the lidar–photometer comparisons with respect to the two sunphotometers ones. Such a behaviour is confirmed by the linear regression analysis which finds a correlation coefficient $r=0.76$ between the two sunphotometers data sets and $r=0.88$ – 0.90 when comparing lidar (either model) to observations of both sunphotometers.

These comparisons of lidar-estimated AOD against direct measurements show that both aerosol models employed to invert the lidar signal provide good results in terms of integral aerosol optical depth, with maximum combined errors of the order of 19–24%. However, a net improvement is observed when the inversion scheme considers the nonsphericity of the scatterers. In this case, the lidar and sunphotometer performance can be considered as equivalent and combined relative errors lower down to the range 12–22%. These results also support the reliability of the vertical profiles of maritime and desert dust aerosol extinction obtained by means of the nonspherical dust model during PAUR II (Gobbi et al., 2000).

Acknowledgements

This work has been carried out under the European Union contract ENV4-CT97-0623, “PAUR II”, coordinated by Professor C. Zerefos of the University of Thessaloniki, Greece.

References

- Ansmann, A., Riebesell, M., Wandinger, U., Weitkamp, C., Voss, E., Lahmann, W., Michaelis, W., 1992. Combined Raman elastic-backscatter lidar for vertical profiling of moisture, aerosol extinction, backscatter and lidar ratio. *Applied Physics B* 55, 18–28.
- Barnaba, F., Gobbi, G.P., 2001. Lidar estimation of tropospheric aerosol extinction, surface area and volume: maritime and desert dust cases. *Journal of Geophysical Research* 106, 3005–3018.
- Eck, T.F., Holben, B.N., Reid, J., Dubovik, O., Smirnov, A., O'Neill, N.T., Slutsker, I., Kinne, S., 1999. Wavelength dependence of the optical depth of biomass burning, urban, and desert dust aerosols. *Journal of Geophysical Research* 104, 31333–31350.
- Gobbi, G.P., 1995. Lidar estimation of stratospheric aerosol properties: surface, volume, and extinction to backscatter ratio. *Journal of Geophysical Research* 100, 11219–11235.

- Gobbi, G.P., 1998. Polarization lidar returns from aerosols and thin clouds: a framework for the analysis. *Applied Optics* 37, 5505–5508.
- Gobbi, G.P., Barnaba, F., Giorgi, R., Santacasa, A., 2000. Altitude-resolved properties of a Saharan dust event over the Mediterranean. *Atmospheric Environment* 34, 5119–5127.
- Hansen, J., Sato, M., Lacis, A., Ruedy, R., 1997. The missing climate forcing. *Philosophical Transactions of the Royal Society of London, Series B*, 231–240.
- Holben, B.N., Eck, T.F., Slutsker, I., Tanrè, D., Buis, J.P., Setzer, A., Vermote, E., Reagan, J.A., Kaufman, Y.J., Nakajima, T., Lavenu, F., Jankowiak, I., Smirnov, A., 1998. AERONET—a federated instrument network and data archive for aerosol characterization. *Remote Sensing Environment* 66, 1–16.
- Huber, M., Blumthaler, M., Ambach, W., Staehelin, J., 1995. Total atmospheric ozone determined from spectral measurements of direct solar UV irradiance. *Geophysical Research Letters* 22 (1), 53–56.
- Kaufman, Y.J., Tanrè, D., Dubovik, O., Karnieli, A., Remer, L.A., 2001. Absorption of sunlight by dust as inferred from satellite and ground-based remote sensing. *Geophysical Research Letters* 28, 1479–1482.
- Klett, J.D., 1985. Lidar inversion with variable backscatter/extinction ratios. *Applied Optics* 24 (11), 1638–1643.
- Kovalev, V.A., 1995. Sensitivity of the lidar solution to errors of the aerosol backscatter-to-extinction ratio: influence of a monotonic change in the aerosol extinction coefficient. *Applied Optics* 34, 3457–3462.
- Lacis, A., Mishchenko, M.I., 1995. Climate forcing, climate sensitivity and climate response: a radiative modeling perspective on atmospheric aerosols. In: Charlson, M.I., Heintzenberg, M.I. (Eds.), *Aerosol Forcing of Climate*. Wiley, New York, 416 pp.
- Liao, H., Seinfeld, J.H., 1998. Radiative forcing by mineral dust aerosols: sensitivity to key variables. *Journal of Geophysical Research* 103, 31637–31645.
- Measures, R.M., 1984. *Laser Remote Sensing*. Wiley, New York, 510 pp.
- Mishchenko, M.I., Travis, L.D., Kahn, R.A., West, R.A., 1997. Modeling phase functions for dustlike tropospheric aerosols using a shape mixture of randomly oriented polydisperse spheroids. *Journal of Geophysical Research* 102, 16831–16847.
- Piironen, P., Eloranta, E.W., 1994. Demonstration of a high-spectral-resolution lidar based on a Iodine absorption filter. *Optics Letters* 19, 234–236.
- Quijano, A.L., Sokolik, I.N., Toon, O.B., 2000. Radiative heating rates and direct radiative forcing by mineral dust in cloudy atmospheric conditions. *Journal of Geophysical Research* 105, 12207–12219.
- Sokolik, I.N., Toon, O.B., 1996. Direct radiative forcing by anthropogenic airborne mineral aerosols. *Nature* 381, 681–683.